

---

# ANYSR: REALIZING IMAGE SUPER-RESOLUTION AS ANY-SCALE, ANY-RESOURCE

---

**Wengyi Zhan**  
Xiamen University  
Xiamen, China  
zhanwy@stu.xmu.edu.cn

**Mingbao Lin**  
Skywork AI  
Singapore  
linmb001@outlook.com

**Chia-Wen Lin**  
National Tsing Hua University  
Hsinchu, Taiwan  
cwlin@ee.nthu.edu.tw

**Rongrong Ji**  
Xiamen University  
Xiamen, China  
rrji@xmu.edu.cn

## ABSTRACT

In an effort to improve the efficiency and scalability of single-image super-resolution (SISR) applications, we introduce AnySR, to rebuild existing arbitrary-scale SR methods into any-scale, any-resource implementation. As a contrast to off-the-shelf methods that solve SR tasks across various scales with the same computing costs, our AnySR innovates in: 1) building arbitrary-scale tasks as any-resource implementation, reducing resource requirements for smaller scales without additional parameters; 2) enhancing any-scale performance in a feature-interweaving fashion, inserting scale pairs into features at regular intervals and ensuring correct feature/scale processing. The efficacy of our AnySR is fully demonstrated by rebuilding most existing arbitrary-scale SISR methods and validating on five popular SISR test datasets. The results show that our AnySR implements SISR tasks in a computing-more-efficient fashion, and performs on par with existing arbitrary-scale SISR methods. For the first time, we realize SISR tasks as not only any-scale in literature, but also as any-resource. Code is available at <https://github.com/CrispyFeSo4/AnySR>.

**Keywords** Super-Resolution · Any-Scale · Any-Resource

## 1 Introduction

Single image super-resolution (SISR) is the process of reconstructing a low-resolution (LR) image into a high-resolution (HR) one rich in detail. The ill-posed nature has made SISR one of the most challenging tasks in low-level computer vision. The past decades have witnessed the advent of many classic studies that continuously address such a challenge. Typical works such as EDSR [1], RCAN [2], and RDN [3], serving as network backbones, effectively extract both texture and semantic information from LR images and lay the foundation for HR reconstruction. The pixel-shuffle upsampling method [4] takes a step further to enhance the image reconstruction quality. Standing upon the shoulders of these pioneering works, the majority of SISR methods [1, 2, 3] adheres to a straightforward and efficient paradigm in which features are extracted by feature extractors, followed by upscaling modules for reconstruction.

Albeit the encouraging achievement, most of the above methods are confined to addressing the image reconstruction of a fixed upsampling scale and are therefore stuck in repeatedly rebuilding an SR network when the fully trained model cannot accommodate the resolutions in demand. Actually, there is a significant demand for multi-scale SR tasks. Training individual models for respective resolutions seems to be a great waste of computing resources and fails to adapt to real-time online deployment. Reflecting on this, many recent researchers have shifted their focus to integrating any-scale tasks into only one integrated SR model. For example, Meta-SR [9] learns to predict coordinates and scale-oriented convolutional weights to generate HR images. Taking into consideration the neighborhoods in the LR image and a scale-related cell size, the subsequent LIIF [10] utilizes an MLP to predict the pixel values of the queried coordinates in an HR one. To enhance the representational capabilities, LTE [11] further introduces a local texture estimator that transforms coordinate information into the Fourier domain. The very recent SRNO [12] and OPE-SR [13] enable HR tasks of continuous scales by respectively incorporating Neural Operators [14] and introducing an orthogonal position encoding upscale module.

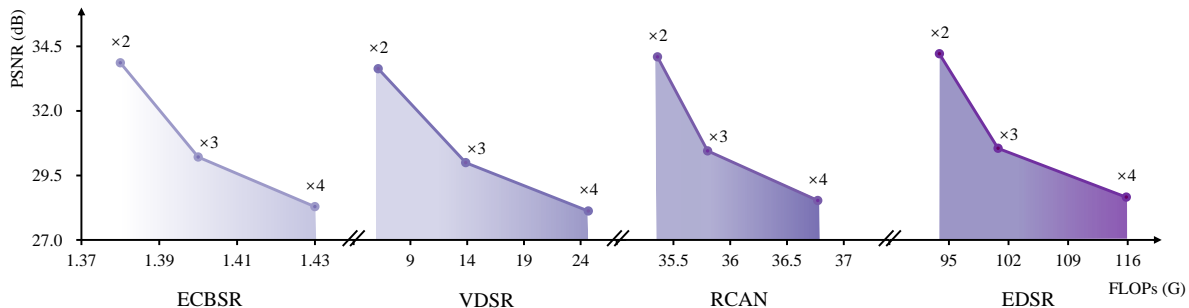


Figure 1: PSNR performance *v.s.* computing cost measured as GFLOPs for existing methods of ECBSR [5], VDSR [6], RCAN [2] and EDSR [1]. For fairness, all reported data is borrowed from [7] and the test set is DIV2K [8].

With the fast development of the computer vision community, more stringent requirements on efficient and scalable vision applications have been put forward [15, 16, 17, 18]. Delving into a reflection on most of the existing arbitrary-scale SR methods, we realize that they are not fully excavated to realize the above advocacy. Though succeeding in tackling SR tasks across various scales in one single network, they also cause additional resource overhead, given our empirical observation that lower-resolution scales can be dealt with more easily. To verify this, we have explicitly conducted an extensive literature review and made a summary in Fig. 1, outlining the performance trend *w.r.t.* the SR scale and network complexity. We can find that a network with relatively lower complexity is sufficient to ensure satisfactory performance for SR tasks with smaller reconstruction scales. For example, when performing a  $\times 2$  SISR task, ECBSR [5] obtains 33.86 dB PSNR with only 1.38 GFLOPs consumption while EDSR [1] achieves a slightly improved performance of 34.21 dB PSNR by eating up totally 93.89 GFLOPs. However, as the scale increases a lot, a more complex network is required for the sake of a better performance. For instance, only 28.29 dB PSNR is gained by the method of ECBSR under 1.43 GFLOPs while the result increases to 28.67 dB PSNR by EDSR when more GFLOPs of 115.83 are taken to construct a  $\times 4$  SISR task.

As analyzed in the existing research [19], the platforms to perform SISR tasks are often featured with limited and varying computing resources over time, due to the potential resource occupation of other applications. On account of the efficiency and scalability of SR applications, more efforts are actually needed to take the edge off computing expenses. As a consequence, we take a step back in this paper and launch the first attempt to realize image super-resolution not only at any-scale in the literature but also with any-resource, which to our best knowledge by far has never been noticed and resolved.

To this end, we propose AnySR in this paper, a general method with “SR” in the method’s name indicating not only Super-Resolution task but also any-Scale and any-Resource implementation. To be more concrete, we reorganize scale information into multiple sub-groups, each of which consists of similar scale sizes. In this context, we construct multiple networks of various complexities so that in situations where computational resources are constrained, lower-complexity ones are distributed to accomplish SISR tasks of smaller scales for the sake of inference efficiency, while higher-complexity ones are oriented to solving higher-scale SISR tasks on account of better performance. Further, to circumvent the introduction of cumbersome parameters, we train and infer all networks in a parameter-sharing manner [20, 21] in which the weights of smaller networks become parts of larger ones. Such a fashion also conveniences the case of abundant computational resources, where opting for the most complex network produces superior reconstruction results for all scales. Importantly, unlike traditional methods [20, 21] that forward a batch of samples multiple times during training, we forward each batch a time and thus do not enlarge the training costs.

Conventional practices have often employed the same feature extraction approach across images of various scales [9, 10]. However, tasks at different scales demand specific adjustments to their features tailored to their respective scales, which can also, to some extent, compensate for the performance loss brought about by reduced computational resources and mutual weight influence from parameter-sharing. For better scale information injection, we enhance any-scale feature in a feature-interweaving fashion, by repeating and inserting scale pairs into features at regular intervals. These operations decouple mutual weight influence and bring “any-scale” implementation closer to the performance of the original arbitrary-scale network. Our AnySR method can be incorporated into most existing arbitrary-scale SR methods, and extensive experiments on typical test datasets have demonstrated its effectiveness.

Overall, the major contributions of this paper are three-fold:

- We present AnySR, a versatile approach designed to adapt existing SISR methods to function seamlessly across “any-scale” and with “any-resources”.
- Any-scale enhancement through feature-interweaving fashion ensures sufficient scale information and correct feature/scale processing.
- Extensive experiments show that when integrated with existing arbitrary-scale SR methods, the proposed AnySR approach consistently achieves comparable performance in a more efficient manner.

## 2 Related Work

### 2.1 Arbitrary-Scale Super-Resolution

Over the past few years, many classic convolutional neural networks (CNNs) based methods, such as SRCNN [22], SRResNet [23], EDSR [1], and RDN [3], have been proposed and shown commendable promise in SR tasks. To further improve SR performance, more methods incorporate residual blocks [24, 6, 25], dense blocks [26, 3, 27], and other techniques [28, 29, 30, 31, 32, 33]. Additionally, certain SR approaches leverage attention mechanisms, such as self-attention [34, 35], channel attention [36, 37, 38], and non-local attention [39, 40, 41]. Yet, most of these methods are tailored to particular scales, constraining their versatility and adaptability.

Therefore, recent researchers have turned their attention to arbitrary-scale SR tasks, aiming to tackle SR problems with arbitrary scales within a unified model. For example, Meta-SR [9] innovatively introduces the first arbitrary-scale meta-upscale module, predicting convolutional filters based on coordinates and scales to generate HR images. Subsequently, employing implicit neural representation, LIIF [10] predicts the RGB value at an arbitrary query coordinate by incorporating image coordinates and features from the backbone around that point. Further enhancements have been achieved by techniques like LTE [11], which introduces a local texture estimator characterizing image textures in Fourier space. Additionally, recent advancements in the SR field have introduced novel structures. For instance, SRNO [12] incorporates Neural Operators, and OPE-SR [13] introduces orthogonal position encoding (OPE), an extension of position encoding. These innovations have demonstrated substantial performance improvements.

### 2.2 Efficient Image Super-Resolution

In recent years, numerous approaches [42, 43, 44, 45, 46] have emerged to develop efficient super-resolution networks. Building upon the pioneering work of SRCNN [22], FSRCNN [42] substantially accelerates the SISR networks. This acceleration is achieved by taking the original LR image as input without bicubic interpolation, using smaller sizes of convolution kernels, and incorporating a deconvolutional layer at the final stage of the network for upsampling. LapSRN [47] incrementally reconstructs the sub-band residuals of HR images through the utilization of the Laplacian pyramid. CARN [43] achieves improved efficiency by ingeniously designing cascading residual networks with group convolution. IMDN [48] presents information multi-distillation blocks featuring a contrast-aware channel attention layer. In parallel, RFDN [44] optimizes the architecture using a feature distillation mechanism through the proposed residual feature distillation block. In the wake of RFDN, RLFN [49] adds more channels to compensate for discarded feature distillation branches and introduces the residual local feature block, resulting in enhanced inference speed and superior performance with fewer parameters. On the other hand, FMEN [45] introduces the re-parameterization technique, expanding the optimization space during training through re-parameterizable building blocks [50], without incurring additional inference time.

## 3 Methodology

### 3.1 Preliminaries

The general pipeline of our AnySR method acts in accordance with most existing methods [1, 51, 38] as in the upper half of Fig. 2, typically highlighted with 1) A  $3 \times 3$  convolutional layer to convert a given LR image  $I_{LR} \in \mathbb{R}^{H \times W \times 3}$  into a shallow feature  $f_s \in \mathbb{R}^{H \times W \times C_{in}}$  where  $C_{in}$  represents the channel number. 2)  $N$  consecutive blocks for deep feature extraction, standing out as the “AnySR” block in this paper, along with a common convolutional layer and a global residual connection to the shadow feature  $f_s$ . 3) An upsampler  $U(\cdot)$  to reconstruct an HR version of the LR image, denoted as  $I'_{HR} \in \mathbb{R}^{H' \times W' \times 3}$  where  $H' > H$  and  $W' > W$ . For ease of the following representation, we use  $F(\cdot)$  to denote feature extraction operations in 1) and 2).

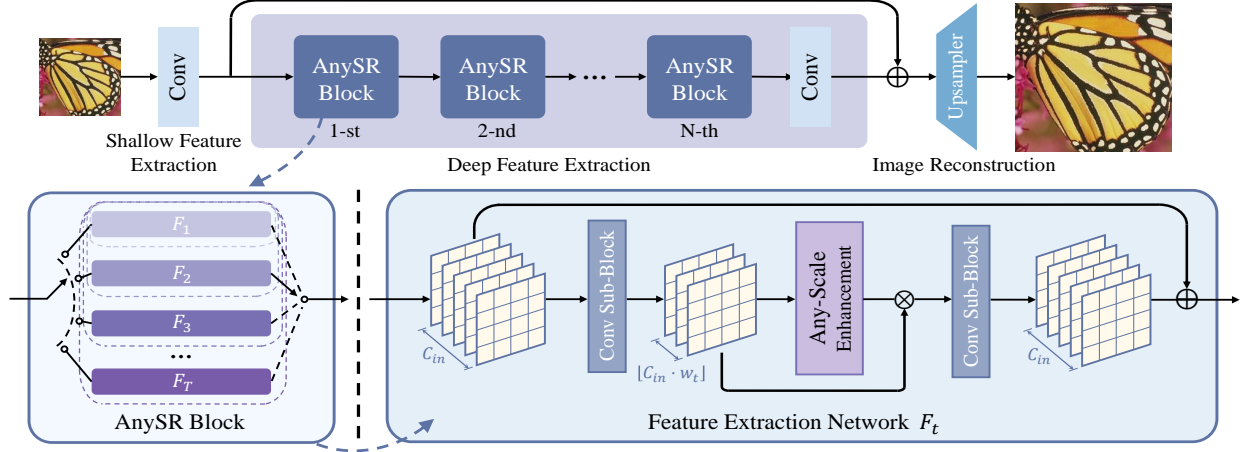


Figure 2: Overview of the proposed AnySR: Includes Shallow Feature Extraction, Deep Feature Extraction with AnySR Blocks, and Image Reconstruction. AnySR Block automatically selects sub-net  $F_t$  based on task complexity for feature extraction and enhancement.

Given an LR image  $I_{LR}$ , the process of constructing its HR version  $I'_{HR}$  under the arbitrary-scale setting [9, 10, 51] can be formulated as

$$I'_{HR} = U(F(I_{LR}, S; \Theta_F); \Theta_U), \quad (1)$$

where  $\Theta_F$  denotes the learnable parameters of feature extractor  $F(\cdot)$ , taking as inputs LR image  $I_{LR}$  and upsampling scale set  $S = \{(s_i^h, s_i^w)\}_{i=1}^n$ ,  $\Theta_U$  denotes the learnable parameters of upsampler  $U(\cdot)$  taking the outputs of  $F(\cdot)$  as inputs.

As analyzed in Sec. 1, such an arbitrary-scale pipeline constrains the efficiency and scalability of applying SR models. A less complex network can sometimes adequately handle a smaller reconstruction scale. Consequently, allocating a uniform inference overhead for all scales manifests insufficient scalability to accommodate running platforms of time-varying computational resources, and presents poor efficiency when dealing with smaller reconstruction scales. Contemplating this, in Sec. 3.2, we rebuild current methods as an implementation of “any-resource”, to enable the selection of a smaller network in the SR model based on the abundance of computing resources. Then, we continue proposing “feature-interweaving” in Sec. 3.3 to enhance the performance under our “any-resource” implementation.

### 3.2 Any-Resource Implementation

The upper part of Fig. 2 manifests our any-resource implementation. Considering the close relationship between scaling factor  $(s_i^h, s_i^w)$  and reconstruction difficulty, we rearrange scale set  $S$  in an ascending order and partition it into  $T$  groups:

$$S_1 \cup S_2 \cup \dots \cup S_T = S \quad \text{and} \quad S_1 \cap S_2 \cap \dots \cap S_T = \emptyset. \quad (2)$$

Correspondingly,  $T$  distinct feature extraction networks  $\{F_t\}_{t=1}^T$  with various complexities are then constructed. Each network  $F_t$  is affiliated with parameters of a particular size as  $\Theta_{F_t}$ , indicating the complexity. We have  $|\Theta_{F_{t+1}}| > |\Theta_{F_t}|$ .

A natural approach is to utilize network  $F_t$  to process the SR tasks within group  $S_t$  such that 1) Smaller-scale tasks can be efficiently fulfilled through a structurally simple network; 2) Larger-scale ones benefit from complex networks. Thus, the process of reconstructing group  $S_t$  tasks becomes

$$I'_{HR} = U(F_t(I_{LR}, S_t; \Theta_{F_t}); \Theta_U). \quad (3)$$

**All-in-One Training.** Although the above process greatly conserves computational resources, it defects in that 1)  $T$  networks have to be repeatedly trained like traditional SR methods, and that 2) additional parameters are introduced compared with arbitrary-scale SR methods. To solve this issue, we follow [20, 21] to train and infer all networks in a parameter-sharing manner by the following set of constraints:

$$\Theta_{F_1} = \Theta_F[1 : |\Theta_{F_1}|], \Theta_{F_2} = \Theta_F[1 : |\Theta_{F_2}|], \dots, \Theta_{F_T} = \Theta_F[1 : |\Theta_{F_T}|] = \Theta_F,$$

where  $\Theta_F[1 : |\Theta_{F_t}|]$  represents the first  $|\Theta_{F_t}|$  filters of  $\Theta_F$ , which indeed makes  $F_t$  a subnet of  $F$  as  $\Theta_{F_1} \subset \Theta_{F_2} \subset \dots \subset \Theta_{F_T} \subseteq \Theta_F$ .

---

**Algorithm 1** AnySR Training.

---

**Input:** LR image  $I_{LR}$ , HR image  $I_{HR}$ , sorted and split scale set  $S = S_1 \cup S_2 \cup \dots \cup S_T$ , a pre-trained arbitrary-scale SR model  $F$  with weights  $\Theta_F$ , training step  $K$ .

- 1: **for**  $k = 1 \rightarrow K$  **do**
- 2:    $t \sim [1, 2, \dots, T]$ ;
- 3:    $(s^h, s^w) \sim S_t$ ;
- 4:    $t \leftarrow T$  with probability  $p$ ;
- 5:   Forward  $I_{LR}$  and  $(s^h, s^w)$  to  $F$  with weights  $\Theta_F[1 : |\Theta_{F_t}|]$ ;
- 6:   Obtain reconstructed HR image  $I'_{HR}$  via Eq. (4);
- 7:    $F \leftarrow F - \beta \nabla \|I_{HR} - I'_{HR}\|_1$ .       % Only  $\Theta_F[1 : |\Theta_{F_t}|]$  are updated.
- 8: **end for**
- 9: **return**  $F$

---

Consequently, the process of our AnySR to reconstruct multiple scales can be unified as follows:

$$I'_{HR} = U(F(I_{LR}, S_t; \Theta_F[1 : |\Theta_{F_t}|]); \Theta_U). \quad (4)$$

Algorithm 1 shows how to train AnySR. At each training iteration, we randomly forward a subnet of the original model  $F$  and update only the corresponding weights  $\Theta_F[1 : |\Theta_{F_t}|]$ . It realizes multiple networks of different resources in one training, and introduces no additional parameters. In Line 4 of Algorithm 1, the subnet is probably reset to  $F$  for the consideration of retaining the original ability of  $F$ , which performs multiple scale tasks through the entire weights  $\Theta_F$ . Note that, we forward each batch once, a distinction from existing weight-sharing methods [20, 21] that perform multiple forwards, for the consideration of 1) better training efficiency, and 2) already fully-pretrained weights  $\Theta_F$ .

### 3.3 Any-Scale Enhancement

Though any-resource implementation boosts the scalability and efficiency of SR tasks, its parameter-sharing puts the performance at risk, due to fewer parameters for smaller scales and mutual weight influence among different scales. It is of great necessity to enhance the reconstruction results of smaller networks and bring them closer to the performance of the original arbitrary-scale network.

Previous research [51] has proven beneficial from linking extracted features with scales, ultimately optimizing the performance of the upsampling module. We realize scale information can be well excavated and ameliorated under our any-resource implementation for the following reasons: 1) The weights  $\Theta_F[1 : |\Theta_{F_t}|]$  are particularly trained to deal with the scale set  $S_t$ , leading to scale-aware features; 2) Partial weights are shared among different subnets, injecting information of other scales. Therefore, we achieve any-scale enhancement by emphasizing the significance of customized handling for features across different scales. Specifically, as shown in Fig. 2, inside each ‘‘AnySR’’ block lies two sub-blocks with the first/second reducing/increasing the channels. We choose to inject better scale information, in a feature-interweaving fashion as illustrated in Fig. 3(a), into the outputs of the first sub-block, denoted as  $f_t \in \mathbb{R}^{H \times W \times (\lfloor C_{in} \cdot w_t \rfloor)}$ , where  $w_t = \frac{|\Theta_{F_t}|}{|\Theta_F|}$ , and  $\lfloor \cdot \rfloor$  denotes the floor function.

**Feature-Interweaving.** Features  $f_t \in \mathbb{R}^{H \times W \times (\lfloor C_{in} \cdot w_t \rfloor)}$  from  $F_t$  would first go through a global average pooling (GAP) to get a variant  $\tilde{f}_t \in \mathbb{R}^{\lfloor C_{in} \cdot w_t \rfloor}$  where the scale information  $(s^h, s^w) \in S_t$  is formally injected.

To this end, one naive fashion, as illustrated in the upper half of Fig. 3(b), is to follow existing methods [10, 52] which simply concatenate  $(s^h, s^w)$  at the rear of  $\tilde{f}_t$  to form  $\bar{f}_t = [\tilde{f}_t, s^h, s^w] \in \mathbb{R}^{\lfloor C_{in} \cdot w_t \rfloor + 2}$ . Then, a two-layer MLP, with weights  $W_1 \in \mathbb{R}^{2 \cdot C_{in} \times (C_{in} + 2)}$ ,  $W_2 \in \mathbb{R}^{C_{in} \times 2 \cdot C_{in}}$  and a ReLU layer inserted between, is created, followed by a Sigmoid function to weight the original features  $f_t$  as

$$f'_t = f_t \odot \text{Sigmoid}(W_2[1 : \lfloor C_{in} \cdot w_t \rfloor, :] \cdot \text{ReLU}(W_1[:, 1 : \lfloor C_{in} \cdot w_t \rfloor + 2] \cdot \bar{f}_t)), \quad (5)$$

where  $W_1[:, 1 : \lfloor C_{in} \cdot w_t \rfloor + 2] \in \mathbb{R}^{2 \cdot C_{in} \times (\lfloor C_{in} \cdot w_t \rfloor + 2)}$  and  $W_2[1 : \lfloor C_{in} \cdot w_t \rfloor, :] \in \mathbb{R}^{\lfloor C_{in} \cdot w_t \rfloor \times 2 \cdot C_{in}}$  are the shared MLP weights for the network  $F_t$ .  $f'_t$  then serves as the input of the second sub-block in the ‘‘AnySR’’ block.

Though this naive approach facilitates the interaction between features and scale information, two notable limitations, as we analyze, arise: 1) Insufficient scale information. Compared to a total of  $\lfloor C_{in} \cdot w_t \rfloor$  channels in image features, where  $\lfloor C_{in} \cdot w_t \rfloor \gg 2$  signifies a limited influence of scale information on the weighted features, the scale information takes up only 2 dimensions. 2) Inappropriate scale processing. For the MLP weights  $W_1 \in \mathbb{R}^{2 \cdot C_{in} \times (C_{in} + 2)}$ , the sub-weights  $W_1[:, \lfloor C_{in} \cdot w_t \rfloor + 1 : \lfloor C_{in} \cdot w_t \rfloor + 2] \in \mathbb{R}^{2 \cdot C_{in} \times 2}$  are used to process the scale information  $(s^h, s^w) \in S_t$ . For  $(s^h, s^w) \in S_{t+1}$ , the weights to process scales are  $W_1[:, \lfloor C_{in} \cdot w_{t+1} \rfloor + 1 : \lfloor C_{in} \cdot w_{t+1} \rfloor + 2] \in \mathbb{R}^{2 \cdot C_{in} \times 2}$  and

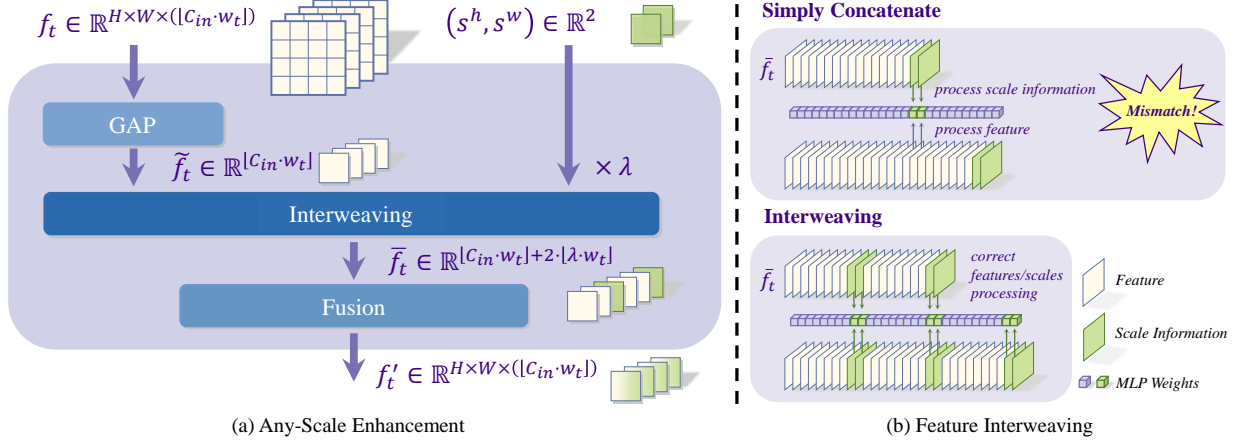


Figure 3: Framework of our any-scale enhancement including (a) any-scale enhancement pipeline and (b) feature-interweaving illustration.

$W_1[:, [C_{in} \cdot w_t] + 1 : [C_{in} \cdot w_t] + 2] \in \mathbb{R}^{2 \cdot C_{in} \times 2}$  are now responsible for processing image features. If off-the-shelf methods [10, 52] are still applied here, as a result, they may weaken the impact of scale information and thus fail to well excavate customized features at different scales. Experimental demonstration has been provided in Table 4.

To better align features with scale information, for network  $F_t$ , our feature-interweaving inserts scale pair  $(s^h, s^w)$  for  $\lambda$  times into positions  $([C_{in} \cdot i/\lambda] + 2i - 1, [C_{in} \cdot i/\lambda] + 2i)$  where  $i = 1, 2, \dots, [\lambda \cdot w_t]$ , of the pooled features  $\tilde{f}_t \in \mathbb{R}^{C_{in} \cdot w_t}$ , which leads to the following concatenated features  $\tilde{f}_t \in \mathbb{R}^{[C_{in} \cdot w_t] + 2 \cdot [\lambda \cdot w_t]}$ :

$$\begin{aligned} \tilde{f}_t = & \left[ \tilde{f}_t[1 : [C_{in} \cdot 1/\lambda]], s^h, s^w, \tilde{f}_t[[C_{in} \cdot 1/\lambda] + 1 : [C_{in} \cdot 2/\lambda]], s^h, s^w, \dots, \right. \\ & \left. \tilde{f}_t[[C_{in} \cdot (i-1)/\lambda] + 1 : [C_{in} \cdot i/\lambda]], s^h, s^w, \dots, \tilde{f}_t[[C_{in} \cdot [\lambda \cdot w_t]/\lambda] + 1 : ] \right]. \end{aligned} \quad (6)$$

Then, weights  $W_1$  in the two-layer MLP becomes  $W_1 \in \mathbb{R}^{2 \cdot C_{in} \times (C_{in} + 2 \cdot \lambda)}$ , and the weighted features in (5) becomes:

$$f'_t = f_t \odot \text{Sigmoid}(W_2[1 : [C_{in} \cdot w_t], :]) \cdot \text{ReLU}(W_1[:, 1 : [C_{in} \cdot w_t] + 2 \cdot [\lambda \cdot w_t]] \cdot \tilde{f}_t). \quad (7)$$

As a consequence, the weights  $W_1[:, [C_{in} \cdot i/\lambda] + 2i - 1 : [C_{in} \cdot i/\lambda] + 2i] \in \mathbb{R}^{2 \cdot C_{in} \times 2}$ , in which  $i = 1, 2, \dots, [\lambda \cdot w_t]$  consistently deal with the scale information whatever the specific value of  $t$ . In conclusion, our feature-interweaving overcomes the issues of traditional methods [10, 52] by taking into account two key operations: 1) repeating the scale pair  $(s^h, s^w)$   $\lambda$  times to ensure sufficient scale information for network  $F_t$ ; 2) inserting scale pairs into features in regular intervals to ensure the correct feature/scale processing. The efficacy of our feature-interweaving will be shown in Sec. 4.

## 4 Experimental Results

### 4.1 Experiment Settings

**Training Details.** We primarily rely on existing well-established arbitrary-scale SR models, including Meta-SR [9], LIIF [10], ArbSR [51], and SRNO [12], for AnySR rebuilding. Without loss of generality, experiments on top of two famous feature extraction backbones, including EDSR [1] and RDN [3], are conducted to validate the universality of our AnySR. During specific implementation, we configure the network number  $T = 4$  and  $\{w_i\}_{i=1}^T = \{0.5, 0.7, 0.9, 1.0\}$ , that is, the smallest scale group  $S_1$  enables a reduction in inference cost by up to 50% compared with the original. The reset probability  $p$  in Line 4 of Algorithm 1 is configured at 0.6, and the hyper-parameter  $\lambda$  in feature-interweaving is set as 4 for EDSR and 8 for RDN. Accordingly, the scale groups  $\mathcal{S}_1 = \{1.1, 1.2, \dots, 1.7\}$ ,  $\mathcal{S}_2 = \{1.8, 1.9, \dots, 2.5\}$ ,  $\mathcal{S}_3 = \{2.6, 2.7, \dots, 3.2\}$  and  $\mathcal{S}_4 = \{3.3, 3.4, \dots, 4.0\}$ . To ensure a fair performance evaluation, we keep identical settings and configurations used for the original models in our training process. The patch size is  $50 \times 50$  for Meta-SR and ArbSR,  $48 \times 48$  for LIIF, and  $128 \times 128$  for SRNO, with a batch size of 8 per GPU for EDSR and 4 per GPU for

Table 1: PSNR (dB) of existing arbitrary-scale SR methods and their AnySR variants (through different subnets) highlighted by †. The \* indicates our re-implementation. Following [13], we highlight AnySR performance by blue if less than 0.15db of the vanilla method, and red if better.

Backbone Networks	Methods	Set5 [53]			Set14 [54]			B100 [55]			Urban100 [56]			Manga109 [57]		
		×2	×3	×4	×2	×3	×4	×2	×3	×4	×2	×3	×4	×2	×3	×4
EDSR	MetaSR*	37.89	34.35	32.08	33.57	30.29	28.52	32.14	29.07	27.54	32.07	28.10	25.97	38.36	33.39	30.37
	MetaSR†	<b>37.85</b>	<b>34.40</b>	<b>32.17</b>	<b>33.44</b>	<b>30.28</b>	<b>28.55</b>	<b>32.07</b>	<b>29.06</b>	<b>27.56</b>	31.84	<b>28.09</b>	<b>26.05</b>	<b>38.30</b>	<b>33.47</b>	<b>30.46</b>
	LIIF	37.99	34.40	32.24	33.66	30.34	28.62	32.17	29.10	27.60	32.15	28.22	26.15	36.19	31.47	28.81
	LIIF†	<b>37.88</b>	<b>34.34</b>	<b>32.21</b>	<b>33.53</b>	<b>30.32</b>	<b>28.61</b>	<b>32.10</b>	<b>29.08</b>	<b>27.59</b>	31.90	<b>28.21</b>	<b>26.19</b>	35.99	<b>31.45</b>	<b>28.80</b>
	ArbSR*	37.97	34.39	32.07	33.70	30.31	28.56	32.19	29.11	27.55	32.18	28.13	25.96	38.52	33.63	30.46
	ArbSR†	<b>37.87</b>	<b>34.34</b>	<b>32.05</b>	33.46	<b>30.28</b>	<b>28.53</b>	<b>32.10</b>	<b>29.07</b>	<b>27.53</b>	31.73	<b>27.99</b>	<b>25.92</b>	38.33	<b>33.53</b>	<b>30.35</b>
	SRNO	38.15	34.53	32.39	33.83	30.50	28.79	32.27	29.29	27.67	32.63	28.58	26.50	39.01	33.91	30.88
	SRNO†	<b>38.04</b>	<b>34.50</b>	<b>32.38</b>	<b>33.74</b>	<b>30.47</b>	<b>28.78</b>	<b>32.19</b>	<b>29.15</b>	<b>27.64</b>	32.27	<b>28.45</b>	<b>26.45</b>	38.78	<b>33.77</b>	<b>30.83</b>
RDN	MetaSR	38.22	34.63	32.38	33.98	30.54	28.78	32.33	29.26	27.71	32.92	28.82	26.55	39.18	34.14	31.03
	MetaSR†	<b>38.13</b>	<b>34.57</b>	<b>32.51</b>	<b>33.94</b>	<b>30.50</b>	<b>28.83</b>	<b>32.25</b>	<b>29.21</b>	<b>27.74</b>	32.69	28.63	<b>26.69</b>	<b>39.06</b>	<b>34.07</b>	<b>31.27</b>
	LIIF	38.17	34.68	32.50	33.97	30.53	28.80	32.32	29.26	27.74	32.87	28.82	26.68	39.26	34.21	31.20
	LIIF†	<b>38.15</b>	<b>34.58</b>	<b>32.49</b>	<b>33.84</b>	<b>30.49</b>	<b>28.82</b>	<b>32.27</b>	<b>29.21</b>	<b>27.74</b>	32.59	28.62	<b>26.68</b>	39.02	34.02	<b>31.22</b>
	ArbSR*	38.10	34.57	32.26	33.83	30.46	28.68	32.26	29.19	27.64	32.47	28.45	26.23	38.81	34.02	30.87
	ArbSR†	<b>38.01</b>	<b>34.43</b>	<b>32.31</b>	33.61	<b>30.37</b>	<b>28.70</b>	<b>32.17</b>	<b>29.11</b>	<b>27.66</b>	32.13	28.14	<b>26.30</b>	38.61	33.70	<b>30.94</b>
	SRNO	38.32	34.84	32.69	34.27	30.71	28.97	32.43	29.37	27.83	33.33	29.14	26.98	39.47	34.62	31.58
	SRNO†	<b>38.18</b>	<b>34.73</b>	<b>32.72</b>	34.03	<b>30.60</b>	<b>28.98</b>	<b>32.33</b>	<b>29.27</b>	<b>27.81</b>	32.94	28.87	<b>26.95</b>	39.25	34.33	<b>31.53</b>

RDN. We train AnySR for 500 epochs from the pre-trained models, with an initial learning rate  $10^{-5}$  decayed by 0.5 every 200 epochs. We employ an  $\ell_1$  loss [1] and the Adam optimizer [58].

**Dataset.** For training, current practices [38] use DF2K (including DIV2K [8] and Flickr2K [59]) as the training set, or pre-training on ImageNet1K [60] to enhance performance. For fairness, we start directly from the pre-trained models already applied with these techniques and focus solely on retraining with the DIV2K dataset.

For evaluation, we assess the PSNR on the most common evaluation datasets in the literature, including Set5 [53], Set14 [54], B100 [61], Urban100 [56], Manga109 [57].

## 4.2 Main Results

**Quantitative Results.** Table 1 and Table 2 show the PSNR performances of off-the-shelf arbitrary-scale methods, compared to that of AnySR variants with different subnets dealing with individual scales and that of AnySR-retrained largest network for all scales. Fig. 4 presents a bar graph detailing the PSNR performances across all 30 scales ( $\times 1.1 \sim \times 4.0$ ) for the three entities mentioned above. Considering the unavailability of some existing models (Meta-SR: EDSR; ArbSR: EDSR, RDN), we re-implement and re-train them following the experiment settings outlined in the papers [9, 51].

In Table 1, our AnySR approach markedly decreases computational expenses while preserving visual qualities, thereby improving network efficiency and scalability. In particular, when selecting the subnetwork for inference, there is an average performance drop of 0.15 dB on benchmark datasets, primarily observed at smaller scales. Considering the smaller subnetwork reduces computational costs by up to 50%, we find this performance drop acceptable. Additionally, Table 2 shows that, when using the entire network, the average performance drop is only 0.05 dB. This indicates that AnySR-retrained models can effectively preserve the original model’s performance during the rebuilding process, which can also be visually observed in Fig. 4. Such good performance is closely related to the reset probability  $p$  in Line 4 of Algorithm 1, which will be further investigated in Sec. 4.4. Overall, as evidenced by the results, our AnySR succeeds in dynamically selecting the reconstruction network according to the availability of computing resources, thereby making

Table 2: PSNR (dB) of existing arbitrary-scale SR methods and AnySR-retrained version (through the largest network) denoted by †. The \* indicates our re-implementation. Following [13], we highlight AnySR performance by blue if less than 0.15db of the vanilla method, and red if better.

Backbone Networks	Methods	Set5 [53]			Set14 [54]			B100 [55]			Urban100 [56]			Manga109 [57]		
		×2	×3	×4	×2	×3	×4	×2	×3	×4	×2	×3	×4	×2	×3	×4
EDSR	MetaSR*	37.89	34.35	32.08	33.57	30.29	28.52	32.14	29.07	27.54	32.07	28.10	25.97	38.36	33.39	30.37
	MetaSR†	37.89	34.40	32.17	33.58	30.32	28.55	32.14	29.08	27.56	32.16	28.19	26.05	38.41	33.50	30.46
	LIIF	37.99	34.40	32.24	33.66	30.34	28.62	32.17	29.10	27.60	32.15	28.22	26.15	36.19	31.47	28.81
	LIIF†	37.98	34.37	32.21	33.62	30.35	28.61	32.15	29.09	27.59	32.11	28.25	26.19	36.26	31.53	28.80
	ArbSR*	37.97	34.39	32.07	33.70	30.31	28.56	32.19	29.11	27.55	32.18	28.13	25.96	38.52	33.63	30.46
	ArbSR†	37.93	34.35	32.05	33.65	30.30	28.53	32.17	29.08	27.53	32.13	28.07	25.92	38.44	33.60	30.35
	SRNO	38.15	34.53	32.39	33.83	30.50	28.79	32.27	29.29	27.67	32.63	28.58	26.50	39.01	33.91	30.88
	SRNO†	38.12	34.51	32.38	33.81	30.49	28.78	32.25	29.17	27.64	32.52	28.50	26.45	38.96	33.83	30.83
RDN	MetaSR	38.22	34.63	32.38	33.98	30.54	28.78	32.33	29.26	27.71	32.92	28.82	26.55	39.18	34.14	31.03
	MetaSR†	38.19	34.72	32.51	33.94	30.59	28.83	32.30	29.27	27.74	32.94	28.92	26.69	39.23	34.32	31.27
	LIIF	38.17	34.68	32.50	33.97	30.53	28.80	32.32	29.26	27.74	32.87	28.82	26.68	39.26	34.21	31.20
	LIIF†	38.19	34.66	32.49	33.99	30.54	28.82	32.31	29.27	27.74	32.79	28.81	26.68	39.19	34.20	31.22
	ArbSR*	38.10	34.57	32.26	33.83	30.46	28.68	32.26	29.19	27.64	32.47	28.45	26.23	38.81	34.02	30.87
	ArbSR†	38.05	34.59	32.31	33.80	30.47	28.70	32.27	29.20	27.66	32.57	28.52	26.30	38.82	34.01	30.94
	SRNO	38.32	34.84	32.69	34.27	30.71	28.97	32.43	29.37	27.83	33.33	29.14	26.98	39.47	34.62	31.58
	SRNO†	38.27	34.83	32.72	34.23	30.69	28.98	32.39	29.34	27.81	33.23	29.10	26.95	39.43	34.58	31.53

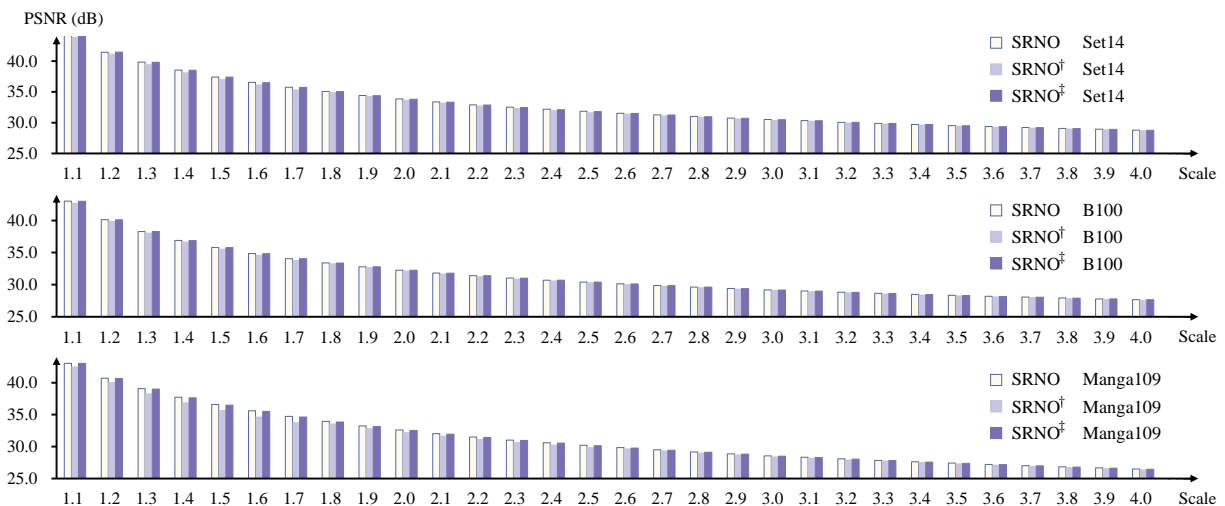


Figure 4: PSNR(dB) comparisons across all scales on different datasets of arbitrary-scale SR model SRNO [12], its AnySR variants (through different subnets) highlighted by †, and AnySR-retrained version (through the largest network) denoted by ‡.

better use of time-varying resources. Further details regarding network complexity will be explicitly discussed in Sec. 4.3.



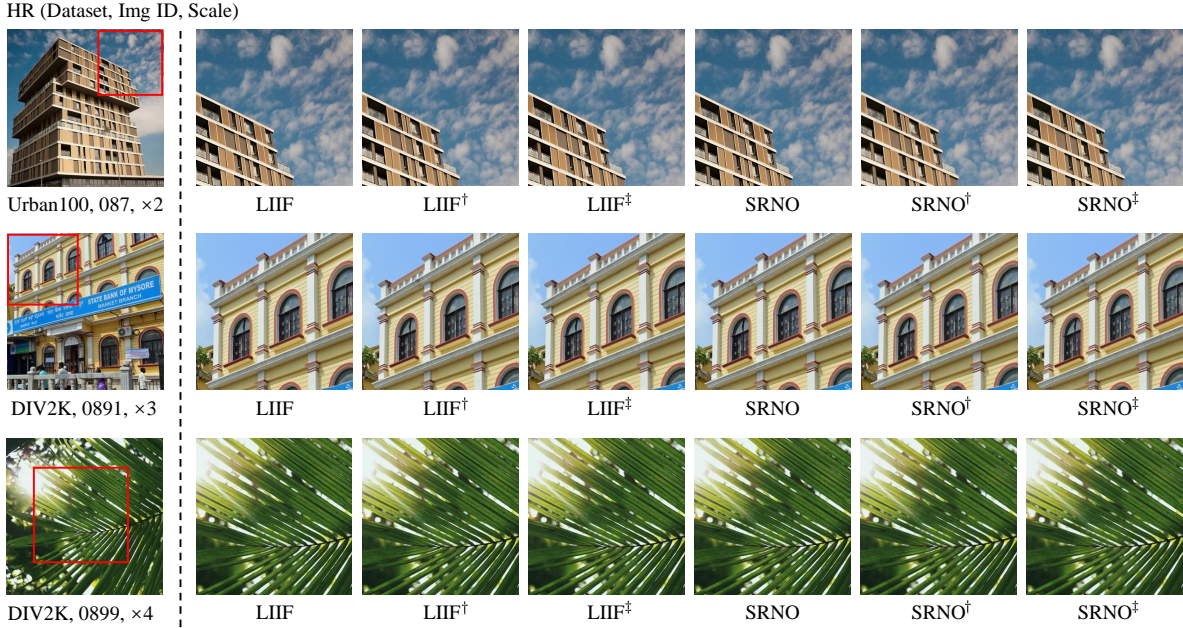


Figure 5: Visualization of existing arbitrary-scale SR models LIIF [10], SRNO [12], their AnySR variants (through different subnets) highlighted by  $\dagger$ , and AnySR-retrained version (through the largest network) denoted as  $\ddagger$ .

Table 3: Comparison of the numbers of Parameters, PSNR performances, and FLOPs counts for SRNO [12] and its AnySR variants (through different subnets) highlighted by  $\dagger$ , AnySR-retrained version (through the largest network) denoted by  $\ddagger$ . Parameters and FLOPs are measured under the setting of consistent pixel size for upsampling SR images on all scales.

Model	Params (M)	$\times 2$		$\times 3$		$\times 4$	
		PSNR (dB)	FLOPs (G)	PSNR (dB)	FLOPs (G)	PSNR (dB)	FLOPs (G)
SRNO	1.22 (100.00%)	33.83 (+0.00)	141.28 (100.00%)	30.50 (+0.00)	62.50 (100.00%)	28.79 (+0.00)	35.28 (100.00%)
SRNO $\dagger$	1.50 (122.95%)	33.74 (-0.09)	97.93 (69.25%)	30.47 (-0.03)	55.54 (88.86%)	28.78 (-0.01)	35.06 (99.39%)
SRNO $\ddagger$	1.50 (122.95%)	33.81 (-0.02)	140.40 (99.27%)	30.49 (-0.01)	62.12 (99.39%)	28.78 (-0.01)	35.06 (99.39%)

**Qualitative Results.** Fig. 5 compares the qualitative performances of LIIF [10], SRNO [12] and their corresponding AnySR variants on DIV2K [8] and Urban100 [56] under two different settings, *i.e.*, different subnets to solve different scales and the entire network to solve all scales.

We show AnySR’s competitive visual quality against others, as there is little noticeable difference in the results. Notably, in the case of  $\times 2$  scale, our method yields impressive visual qualities with substantially reduced computational overhead. From the visual results, it is noticeable that while AnySR $\dagger$  exhibits slight deficiencies in saturation and spatial perception, the overall performance is commendable. The results with AnySR $\ddagger$  closely resemble the LIIF/SRNO image, featuring clear building edges and rich textural details on the leaves. Both AnySR $\dagger$  and AnySR $\ddagger$  avoid generating artifacts or distortions. Therefore, our AnySR succeeds in rebuilding existing models to fulfill any-scale, any-resolution SR tasks while maintaining performance on par with the original models.

### 4.3 Complexity Analysis

We perform a thorough analysis and comparison on SR tasks at different scales, encompassing the number of parameters, PSNR performance, and FLOPs, for SRNO [12] and its AnySR variants of different subnets to solve different scales and the entire network to solve all scales. All results are evaluated on top of the EDSR [1] backbone network on the Set14 dataset [54] as shown in Table 3.

In terms of parameters, our AnySR variant introduces only 0.28 M additional weights (22.95% of the original 1.22 M parameters), primarily dedicated to any-scale enhancement. In relation to computational costs, when performing

Table 4: Ablations on alternations of AnySR including the “w/o ASE” variant removing any-scale enhancement (ASE) and the “w/o FI” variant replacing feature-interweaving (FI) with a simple concatenation. The  $\dagger$  denotes AnySR variants (through different subnets) and  $\ddagger$  denotes AnySR-retrained version (through the largest network). Underlines indicates the best performance.

Settings	Set5			Set14			B100			Urban100			Manga109		
	$\times 2$	$\times 3$	$\times 4$	$\times 2$	$\times 3$	$\times 4$	$\times 2$	$\times 3$	$\times 4$	$\times 2$	$\times 3$	$\times 4$	$\times 2$	$\times 3$	$\times 4$
AnySR $\dagger$	<u>38.04</u>	34.50	<u>32.38</u>	<u>33.74</u>	<u>30.47</u>	<u>28.78</u>	<u>32.19</u>	<u>29.15</u>	<u>27.64</u>	<u>32.27</u>	<u>28.45</u>	<u>26.45</u>	<u>38.78</u>	<u>33.77</u>	<u>30.83</u>
AnySR $\dagger$ (w/o ASE)	38.01	<u>34.51</u>	32.34	33.72	30.43	28.73	32.14	29.11	27.61	<u>32.27</u>	28.44	26.43	38.70	33.74	30.79
AnySR $\dagger$ (w/o FI)	38.00	34.47	32.33	33.71	30.42	28.73	32.14	29.12	27.61	32.25	28.43	26.42	38.75	33.72	30.81
AnySR $\ddagger$	<u>38.12</u>	34.51	<u>32.38</u>	<u>33.81</u>	<u>30.49</u>	<u>28.78</u>	<u>32.25</u>	<u>29.17</u>	<u>27.64</u>	<u>32.52</u>	<u>28.50</u>	<u>26.45</u>	<u>38.96</u>	<u>33.83</u>	<u>30.83</u>
AnySR $\ddagger$ (w/o ASE)	38.10	<u>34.52</u>	32.34	33.76	30.45	28.73	32.21	29.12	27.61	32.51	28.47	26.43	38.90	33.81	30.79
AnySR $\ddagger$ (w/o FI)	38.10	34.48	32.33	33.76	30.45	28.73	32.22	29.14	27.61	32.50	28.46	26.42	38.91	33.80	30.81

Table 5: Ablations on the reset probability  $p$ . The  $\ddagger$  denotes AnySR-retrained version (through the largest network). Underlines indicates the best performance.

Settings	Set5			Set14			B100			Urban100			Manga109		
	$\times 2$	$\times 3$	$\times 4$	$\times 2$	$\times 3$	$\times 4$	$\times 2$	$\times 3$	$\times 4$	$\times 2$	$\times 3$	$\times 4$	$\times 2$	$\times 3$	$\times 4$
AnySR $\ddagger$ ( $p=0$ )	38.06	34.47	32.37	33.76	30.46	28.77	32.21	29.14	27.64	32.48	28.46	26.44	38.91	33.82	30.82
AnySR $\ddagger$ ( $p=0.2$ )	38.07	34.47	32.37	33.78	30.46	28.76	32.22	29.14	27.64	32.50	28.47	<u>26.45</u>	38.93	33.83	30.82
AnySR $\ddagger$ ( $p=0.4$ )	38.08	34.48	32.37	33.78	30.46	28.77	32.22	29.14	<u>27.65</u>	32.50	28.47	26.44	38.94	33.83	<u>30.83</u>
AnySR $\ddagger$ ( $p=0.6$ )	<u>38.12</u>	<u>34.51</u>	<u>32.38</u>	<u>33.81</u>	<u>30.49</u>	<u>28.78</u>	<u>32.25</u>	<u>29.17</u>	<u>27.65</u>	<u>32.52</u>	<u>28.50</u>	<u>26.45</u>	<u>38.96</u>	<u>33.83</u>	<u>30.83</u>
AnySR $\ddagger$ ( $p=0.8$ )	38.11	<u>34.51</u>	<u>32.38</u>	33.80	<u>30.49</u>	28.77	32.24	29.16	<u>27.65</u>	32.51	28.49	<u>26.45</u>	<u>38.96</u>	<u>33.84</u>	30.82

the  $\times 2$  task with chosen subnetworks, the total number of FLOPs (97.93 G), constitutes only 69.25% of the original 141.28 G. This results in a minimal performance loss of 0.09 dB, making it particularly suitable for devices with limited computational power. In the presence of ample computing resources, AnySR sustains an excellent performance-consumption balance on the original basis. Specifically, the results with AnySR $\ddagger$  in Table 3 across three scales reveal that the FLOPs make up only 99.27%, 99.39%, 99.39% of the original model, though accompanied by a negligible PSNR drop of 0.01~0.02 dB.

In summary, our AnySR is crafted as an inference-efficient method, facilitating efficient deployment on devices with time-varying resources while maintaining good performance, as demonstrated by extensive experiments.

#### 4.4 Ablation Studies

We conduct ablation studies to validate the effectiveness of individual components of AnySR. All ablation experiments are performed on SRNO [12], using EDSR [1] as the backbone. We compare our AnySR with two variants: 1) “w/o ASE”: AnySR without any-scale enhancement; 2) “w/o FI”: AnySR replacing feature-interweaving with a simple concatenation. Also, we vary the value of reset probability  $p$  in Line 4 of Algorithm 1, to show its importance.

**Any-Scale Enhancement.** Any-scale enhancement constitutes one of the fundamental branches encompassed within our overarching research framework. By injecting, excavating, and ameliorating sufficient scale information, we realize customized handling for features at different scales. In order to validate the effectiveness of ASE, we train the network by removing this component, and the results are presented in Table 4. It is evident that the absence of ASE (*i.e.*, “w/o ASE”) leads to a certain performance drop.

**Feature-Interweaving.** Feature-interweaving considers the non-uniformity of shared weights and overcomes the mutual weight influence across different scales by repeating and inserting scale pairs into features at regular intervals. We study the contribution of this mechanism by substituting the feature-interweaving fashion with a simple concatenation in earlier methods [10, 52]. By introducing feature-interweaving, a better performance is achieved in Table 4.

**Reset Probability  $p$ .** As mentioned in Sec. 3.2, we reset subnet  $F_t$  to the entire network  $F$  with a certain probability  $p$  to retain the original ability. We conduct ablation experiments with different values of  $p = \{0, 0.2, 0.4, 0.6, 0.8\}$ . experimental groups. Note that  $p = 0$  indicates the removal of the reset mechanism. The results are presented in Table 5. A low  $p$ , in particular for  $p = 0$ , leads to minimal impact on enhancing the performance of the entire network during inference. Hence, opting for  $p = 0.6$  or  $0.8$  is deemed more appropriate. Nevertheless, it is observed that with  $p = 0.8$ , the performance improvement for the entire network inference is slightly higher than  $p = 0.6$ , and a higher probability incurs higher training costs. Considering the trade-off between the performance of the entire network inference and network training costs, we ultimately select  $p = 0.6$  as the experimental setting for the study presented in this paper.

## 5 Conclusion and Future Work

In this paper, we presented AnySR, a simple yet versatile approach to transform existing arbitrary-scale super-resolution methods into implementations that adapt to any scale and resource availability. By rebuilding arbitrary-scale tasks into an any-resource implementation, we enable the completion of smaller-scale SISR tasks with reduced computational resources and no additional parameters. To maintain performance, we enhance any-scale features through a feature-interweaving fashion, ensuring sufficient scale information and correct feature/scale processing. Extensive experiments on benchmark datasets demonstrate the efficiency and scalability of our AnySR method in arbitrary-scale SISR applications.

An alternative approach is resorting to a more complex NAS (Neural Architecture Search), which may achieve better performance and will be our major future exploration.

## References

- [1] Bee Lim, Sanghyun Son, Heewon Kim, Seungjun Nah, and Kyoung Mu Lee. Enhanced deep residual networks for single image super-resolution. In *Proc. IEEE/CVF Conf. Comput. Vis. Pattern Recognit. Workshops*, 2017.
- [2] Yulun Zhang, Kunpeng Li, Kai Li, Lichen Wang, Bineng Zhong, and Yun Fu. Image super-resolution using very deep residual channel attention networks. In *Proc. European Conf. Comput. Vis.*, 2018.
- [3] Yulun Zhang, Yapeng Tian, Yu Kong, Bineng Zhong, and Yun Fu. Residual dense network for image super-resolution. In *Proc. IEEE/CVF Conf. Comput. Vis. Pattern Recognit.*, 2018.
- [4] Wenzhe Shi, Jose Caballero, Ferenc Huszár, Johannes Totz, Andrew P Aitken, Rob Bishop, Daniel Rueckert, and Zehan Wang. Real-time single image and video super-resolution using an efficient sub-pixel convolutional neural network. In *Proc. IEEE/CVF Conf. Comput. Vis. Pattern Recognit.*, 2016.
- [5] Xindong Zhang, Hui Zeng, and Lei Zhang. Edge-oriented convolution block for real-time super resolution on mobile devices. In *ACM Conf. Multimedia*, 2021.
- [6] Jiwon Kim, Jung Kwon Lee, and Kyoung Mu Lee. Accurate image super-resolution using very deep convolutional networks. In *Proc. IEEE/CVF Conf. Comput. Vis. Pattern Recognit.*, 2016.
- [7] Shizun Wang, Jiaming Liu, Kaixin Chen, Xiaoqi Li, Ming Lu, and Yandong Guo. Adaptive patch exiting for scalable single image super-resolution. In *Proc. European Conf. Comput. Vis.*, 2022.
- [8] Eirikur Agustsson and Radu Timofte. Ntire 2017 challenge on single image super-resolution: Dataset and study. In *Proc. IEEE/CVF Conf. Comput. Vis. Pattern Recognit. Workshops*, 2017.
- [9] Xuecai Hu, Haoyuan Mu, Xiangyu Zhang, Zilei Wang, Tieniu Tan, and Jian Sun. Meta-sr: A magnification-arbitrary network for super-resolution. In *Proc. IEEE/CVF Conf. Comput. Vis. Pattern Recognit.*, 2019.
- [10] Yinbo Chen, Sifei Liu, and Xiaolong Wang. Learning continuous image representation with local implicit image function. In *Proc. IEEE/CVF Conf. Comput. Vis. Pattern Recognit.*, 2021.
- [11] Jaewon Lee and Kyong Hwan Jin. Local texture estimator for implicit representation function. In *Proc. IEEE/CVF Conf. Comput. Vis. Pattern Recognit.*, 2022.
- [12] Min Wei and Xuesong Zhang. Super-resolution neural operator. In *Proc. IEEE/CVF Conf. Comput. Vis. Pattern Recognit.*, 2023.
- [13] Gaochao Song, Qian Sun, Luo Zhang, Ran Su, Jianfeng Shi, and Ying He. Ope-sr: Orthogonal position encoding for designing a parameter-free upsampling module in arbitrary-scale image super-resolution. In *Proc. IEEE/CVF Conf. Comput. Vis. Pattern Recognit.*, 2023.

- [14] Nikola Kovachki, Zongyi Li, Burigede Liu, Kamyar Azizzadenesheli, Kaushik Bhattacharya, Andrew Stuart, and Anima Anandkumar. Neural operator: Learning maps between function spaces. *arXiv preprint arXiv:2108.08481*, 2021.
- [15] Tailin Liang, John Glossner, Lei Wang, Shaobo Shi, and Xiaotong Zhang. Pruning and quantization for deep neural network acceleration: A survey. *Neurocomputing*, 2021.
- [16] Yizeng Han, Gao Huang, Shiji Song, Le Yang, Honghui Wang, and Yulin Wang. Dynamic neural networks: A survey. *IEEE Trans. Pattern Anal. Mach. Intell.*, 2021.
- [17] Amir Gholami, Sehoon Kim, Zhen Dong, Zhewei Yao, Michael W Mahoney, and Kurt Keutzer. A survey of quantization methods for efficient neural network inference. In *Low-Power Computer Vision (LPCV)*, 2022.
- [18] Gaurav Menghani. Efficient deep learning: A survey on making deep learning models smaller, faster, and better. *ACM Computing Surveys*, 2023.
- [19] Bohong Chen, Mingbao Lin, Kekai Sheng, Mengdan Zhang, Peixian Chen, Ke Li, Liujuan Cao, and Rongrong Ji. Arm: Any-time super-resolution method. In *Eur. Conf. Comput. Vis.*, 2022.
- [20] Yuxin Zhang, Mingbao Lin, Xunchao Li, Han Liu, Guozhi Wang, Fei Chao, Ren Shuai, Yafei Wen, Xiaoxin Chen, and Rongrong Ji. Real-time image demoreing on mobile devices. In *Int. Conf. Learn. Represent.*, 2023.
- [21] Taojiannan Yang, Sijie Zhu, Matias Mendieta, Pu Wang, Ravikumar Balakrishnan, Minwoo Lee, Tao Han, Mubarak Shah, and Chen Chen. Mutualnet: Adaptive convnet via mutual learning from different model configurations. *IEEE Trans. Pattern Anal. Mach. Intell.*, 2021.
- [22] Chao Dong, Chen Change Loy, Kaiming He, and Xiaoou Tang. Image super-resolution using deep convolutional networks. *IEEE Trans. Pattern Anal. Mach. Intell.*, 2016.
- [23] Christian Ledig, Lucas Theis, Ferenc Huszár, Jose Caballero, Andrew Cunningham, Alejandro Acosta, Andrew Aitken, Alykhan Tejani, Johannes Totz, Zehan Wang, et al. Photo-realistic single image super-resolution using a generative adversarial network. In *Proc. IEEE/CVF Conf. Comput. Vis. Pattern Recognit.*, 2017.
- [24] Lukas Cavigelli, Pascal Hager, and Luca Benini. Cas-cnn: A deep convolutional neural network for image compression artifact suppression. In *Proc. Int. Joint Conf. Neural Netw.*, 2017.
- [25] Kai Zhang, Yawei Li, Wangmeng Zuo, Lei Zhang, Luc Van Gool, and Radu Timofte. Plug-and-play image restoration with deep denoiser prior. *IEEE Trans. Pattern Anal. Mach. Intell.*, 2021.
- [26] Xintao Wang, Ke Yu, Shixiang Wu, Jinjin Gu, Yihao Liu, Chao Dong, Yu Qiao, and Chen Change Loy. Esrgan: Enhanced super-resolution generative adversarial networks. In *Proc. European Conf. Comput. Vis. Workshops*, 2018.
- [27] Yulun Zhang, Yapeng Tian, Yu Kong, Bineng Zhong, and Yun Fu. Residual dense network for image restoration. *IEEE Trans. Pattern Anal. Mach. Intell.*, 2020.
- [28] Yunjin Chen and Thomas Pock. Trainable nonlinear reaction diffusion: A flexible framework for fast and effective image restoration. *IEEE Trans. Pattern Anal. Mach. Intell.*, 2016.
- [29] Wenlong Cheng, Mingbo Zhao, Zhiling Ye, and Shuhang Gu. Mfagan: A compression framework for memory-efficient on-device super-resolution gan. *arXiv preprint arXiv:2107.12679*, 2021.
- [30] Xin Deng, Yutong Zhang, Mai Xu, Shuhang Gu, and Yiping Duan. Deep coupled feedback network for joint exposure fusion and image super-resolution. *IEEE Trans. Image Process.*, 2021.
- [31] Xinrui Jiang, Nannan Wang, Jingwei Xin, Keyu Li, Xi Yang, Jie Li, Xiaoyu Wang, and Xinbo Gao. Fabnet: Frequency-aware binarized network for single image super-resolution. *IEEE Trans. Image Process.*, 2023.
- [32] Cheng Ma, Peiqi Yu, Jiwen Lu, and Jie Zhou. Recovering realistic details for magnification-arbitrary image super-resolution. *IEEE Trans. Image Process.*, 2022.
- [33] Qing Cai, Yiming Qian, Jinxing Li, Jun Lyu, Yee-Hong Yang, Feng Wu, and David Zhang. Hippa: Hierarchical patch transformer for single image super resolution. *IEEE Trans. Image Process.*, 2023.
- [34] Jingyun Liang, Jiezhong Cao, Guolei Sun, Kai Zhang, Luc Van Gool, and Radu Timofte. Swinir: Image restoration using swin transformer. In *Int. Conf. Comput. Vis.*, 2021.
- [35] Yi Xiao, Qiangqiang Yuan, Kui Jiang, Jiang He, Chia-Wen Lin, and Liangpei Zhang. Ttst: A top-k token selective transformer for remote sensing image super-resolution. *IEEE Trans. Image Process.*, 2024.
- [36] Tao Dai, Jianrui Cai, Yongbing Zhang, Shu-Tao Xia, and Lei Zhang. Second-order attention network for single image super-resolution. In *Proc. IEEE/CVF Conf. Comput. Vis. Pattern Recognit.*, 2019.

- [37] Ben Niu, Weilei Wen, Wenqi Ren, Xiangde Zhang, Lianping Yang, Shuzhen Wang, Kaihao Zhang, Xiaochun Cao, and Haifeng Shen. Single image super-resolution via a holistic attention network. In *Proc. European Conf. Comput. Vis.*, 2020.
- [38] Xiangyu Chen, Xintao Wang, Jiantao Zhou, Yu Qiao, and Chao Dong. Activating more pixels in image super-resolution transformer. In *Proc. IEEE/CVF Conf. Comput. Vis. Pattern Recognit.*, 2023.
- [39] Ding Liu, Bihan Wen, Yuchen Fan, Chen Change Loy, and Thomas S Huang. Non-local recurrent network for image restoration. In *Adv. Neural Inform. Process. Syst.*, 2018.
- [40] Yiqun Mei, Yuchen Fan, and Yuqian Zhou. Image super-resolution with non-local sparse attention. In *Proc. IEEE/CVF Conf. Comput. Vis. Pattern Recognit.*, 2021.
- [41] Jian-Nan Su, Min Gan, Guang-Yong Chen, Wenzhong Guo, and C. L. Philip Chen. High-similarity-pass attention for single image super-resolution. *IEEE Trans. Image Process.*, 2024.
- [42] Chao Dong, Chen Change Loy, and Xiaoou Tang. Accelerating the super-resolution convolutional neural network. In *Proc. European Conf. Comput. Vis.*, 2016.
- [43] Namhyuk Ahn, Byungkon Kang, and Kyung-Ah Sohn. Fast, accurate, and lightweight super-resolution with cascading residual network. In *Proc. European Conf. Comput. Vis.*, 2018.
- [44] Jie Liu, Jie Tang, and Gangshan Wu. Residual feature distillation network for lightweight image super-resolution. In *Proc. European Conf. Comput. Vis. Workshops*, 2020.
- [45] Zongcai Du, Ding Liu, Jie Liu, Jie Tang, Gangshan Wu, and Lean Fu. Fast and memory-efficient network towards efficient image super-resolution. In *Proc. IEEE/CVF Conf. Comput. Vis. Pattern Recognit.*, 2022.
- [46] Jingyi Zhang, Ziwei Wang, Haoyu Wang, Jie Zhou, and Jiwen Lu. Anycost network quantization for image super-resolution. *IEEE Trans. Image Process.*, 2024.
- [47] Wei-Sheng Lai, Jia-Bin Huang, Narendra Ahuja, and Ming-Hsuan Yang. Deep laplacian pyramid networks for fast and accurate super-resolution. In *Proc. IEEE/CVF Conf. Comput. Vis. Pattern Recognit.*, 2017.
- [48] Zheng Hui, Xinbo Gao, Yunchu Yang, and Xiumei Wang. Lightweight image super-resolution with information multi-distillation network. In *ACM Conf. Multimedia*, 2019.
- [49] Fangyuan Kong, Mingxi Li, Songwei Liu, Ding Liu, Jingwen He, Yang Bai, Fangmin Chen, and Lean Fu. Residual local feature network for efficient super-resolution. In *Proc. IEEE/CVF Conf. Comput. Vis. Pattern Recognit.*, 2022.
- [50] Xiaohan Ding, Xiangyu Zhang, Ningning Ma, Jungong Han, Guiguang Ding, and Jian Sun. Repvgg: Making VGG-style convnets great again. In *Proc. IEEE/CVF Conf. Comput. Vis. Pattern Recognit.*, 2021.
- [51] Longguang Wang, Yingqian Wang, Zaiping Lin, Jungang Yang, Wei An, and Yulan Guo. Learning a single network for scale-arbitrary super-resolution. In *Proc. IEEE/CVF Int. Conf. Comput. Vis.*, 2021.
- [52] Jie Zhang Cao, Qin Wang, Yongqin Xian, Yawei Li, Bingbing Ni, Zhiming Pi, Kai Zhang, Yulun Zhang, Radu Timofte, and Luc Van Gool. Ciaosr: Continuous implicit attention-in-attention network for arbitrary-scale image super-resolution. In *Proc. IEEE/CVF Conf. Comput. Vis. Pattern Recognit.*, 2023.
- [53] Marco Bevilacqua, Aline Roumy, Christine Guillemot, and Marie Line Alberi-Morel. Low-complexity single-image super-resolution based on nonnegative neighbor embedding. In *Proc. British Mach. Vis. Conf.*, 2012.
- [54] Roman Zeyde, Michael Elad, and Matan Protter. On single image scale-up using sparse-representations. In *Proc. Int. Conf. Curves and Surfaces*, 2012.
- [55] David Martin, Charless Fowlkes, Doron Tal, and Jitendra Malik. A database of human segmented natural images and its application to evaluating segmentation algorithms and measuring ecological statistics. In *Proc. IEEE/CVF Int. Conf. Comput. Vis.*, 2001.
- [56] Jia-Bin Huang, Abhishek Singh, and Narendra Ahuja. Single image super-resolution from transformed self-exemplars. In *Proc. IEEE/CVF Conf. Comput. Vis. Pattern Recognit.*, 2015.
- [57] Kiyoharu Aizawa, Azuma Fujimoto, Atsushi Otsubo, Toru Ogawa, Yusuke Matsui, Koki Tsubota, and Hikaru Ikuta. Building a manga dataset “manga109” with annotations for multimedia applications. *IEEE MultiMedia*, 2020.
- [58] Diederik P Kingma and Jimmy Ba. Adam: A method for stochastic optimization. *arXiv preprint arXiv:1412.6980*, 2014.
- [59] Radu Timofte, Eirikur Agustsson, Luc Van Gool, Ming-Hsuan Yang, and Lei Zhang. Ntire 2017 challenge on single image super-resolution: Methods and results. In *Proc. IEEE/CVF Conf. Comput. Vis. Pattern Recognit. Workshops*, 2017.

- [60] Jia Deng, Wei Dong, Richard Socher, Li-Jia Li, Kai Li, and Li Fei-Fei. Imagenet: A large-scale hierarchical image database. In *Proc. IEEE/CVF Conf. Comput. Vis. Pattern Recognit.*, 2009.
- [61] Radu Timofte, Vincent De Smet, and Luc Van Gool. Anchored neighborhood regression for fast example-based super-resolution. In *Proc. IEEE/CVF Int. Conf. Comput. Vis.*, 2013.